Published in final edited form as:
Neuron. 2005 September 15; 47(6): 833–843. doi:10.1016/j.neuron.2005.08.022.

The Pore Helix Dipole Has a Minor Role in Inward Rectifier Channel Function

Franck C. Chatelain[1,3], **Noga Alagem**[2,3], **Qiang Xu**[1], **Raika Pancaroglu**[1], **Eitan Reuveny**[2], and **Daniel L. Minor Jr.**[1,*]

[1]Cardiovascular Research Institute, Departments of Biochemistry and Biophysics and Cellular and Molecular Pharmacology, California Institute for Quantitative Biomedical Research, University of California, San Francisco, Box 2532, San Francisco, California 94143

[2]Department of Biological Chemistry, Weizmann Institute of Science, Rehovot 76100, Israel

Summary

Ion channels lower the energetic barrier for ion passage across cell membranes and enable the generation of bioelectricity. Electrostatic interactions between permeant ions and channel pore helix dipoles have been proposed as a general mechanism for facilitating ion passage. Here, using genetic selections to probe interactions of an exemplar potassium channel blocker, barium, with the inward rectifier Kir2.1, we identify mutants bearing positively charged residues in the potassium channel signature sequence at the pore helix C terminus. We show that these channels are functional, selective, resistant to barium block, and have minimally altered conductance properties. Both the experimental data and model calculations indicate that barium resistance originates from electrostatics. We demonstrate that potassium channel function is remarkably unperturbed when positive charges occur near the permeant ions at a location that should counteract pore helix electrostatic effects. Thus, contrary to accepted models, the pore helix dipole seems to be a minor factor in potassium channel permeation.

Introduction

Electrical signaling is fundamental to the biological processes that drive sensory systems, behavior, and cognition (Kandel et al., 2000). These signals are mediated by membrane proteins known as ion channels that are essential for the generation and propagation of electrical activity (Hille, 2001). A rich diversity of ion channel genes and families that act on a variety of ion types are now known from molecular cloning, genome sequencing, and electrophysiological characterization efforts (Hille, 2001). Regardless of the channel type, facilitation of the transit of ions through the channel and across the cell membrane, a process known as permeation, is a central feature of all ion channels. The hydrophobic core of the lipid bilayer presents a formidable energetic barrier to ion passage (~50 kcal mol^{-1}) (Parsegian, 1969). Interactions between the components of the channel and the permeant ions lower the energy of this barrier substantially (to ~2–3 kcal mol^{-1}) (Berneche and Roux, 2001). This barrier reduction roughly corresponds to a change in the time for an ion to cross the membrane from ~10^{16} years to ~10 ns, such that ion channels allow ion transit across the membrane at rates that are near the diffusion limit. How channels reshape the

*Correspondence: minor@itsa.ucsf.edu.
[3]These authors contributed equally to this work.

Supplemental Data: The Supplemental Data for this article can be found online at http://www.neuron.org/cgi/content/full/47/6/833/DC1/.

transmembrane energetic landscape to facilitate ion passage remains a fundamental question with important implications for understanding ion channel action and for thinking about how molecules that alter channel function, such as drugs that act as blockers, work.

Potassium channels form a large ion channel class (Jan and Jan, 1997) that have attracted great interest and research effort because of two remarkable properties: a high throughput of substrate processing ($\sim 10^8$ ions s^{-1}) accompanied by remarkable substrate fidelity (Doyle et al., 1998; Morais-Cabral et al., 2001). Potassium ion permeation is favored over sodium ions in the range of 1000:1 to 10,000:1 (Hille, 2001). This represents an extraordinary feat since potassium ions are larger than sodium ions (ionic radii of 1.33 Å versus 0.95 Å) (Hille, 2001), and in terms of pore radius alone, any pore that can accommodate potassium ions would readily pass sodium ions. The high-resolution structures of bacterial potassium channels have revealed important architectural principles regarding the molecular design that underlies channel function (Doyle et al., 1998; Jiang et al., 2002, 2003; Kuo et al., 2003). The structure that constitutes the selectivity filter is formed largely by backbone carbonyl groups of the selectivity filter amino acid sequence “TVGYG” that point into the pore. The particular geometric arrangement of these ligands provides an environment that mimics the structural chemistry of the inner hydration shell of potassium ions (Morais-Cabral et al., 2001; Zhou et al., 2001) and together with their local electrostatic properties provides an energetically favorable environment for potassium binding but an unfavorable one for sodium ions (Noskov et al., 2004).

The potassium channel structures also revealed an unexpected architectural feature of the pore, known as the pore helix (Doyle et al., 1998; Jiang et al., 2002, 2003; Kuo et al., 2003). This short α helix precedes the ion selectivity filter, bears part of the most-conserved portion of potassium channels, and points its C terminus toward ions in the permeation pathway. Structural observations suggested a paradigm for ion permeation in which electrostatic interactions between helix dipoles and the permeant ions serve as important contributors to the energetics of channel function (Doyle et al., 1998; Dutzler et al., 2002; Roux and MacKinnon, 1999). Interactions between the permeant ion and dipoles from the pore helices are proposed to lower the electrostatic destabilization that would otherwise occur upon transfer of an ion into the central cavity of the channel, even though the distance between the permeant ions and the dipoles is greater than that normally seen for ion-dipole interactions (Roux and MacKinnon, 1999). Potassium channel pore helices are expected to have counterparts in other members of the cation channel superfamily, such as voltage-gated sodium, voltage-gated calcium, TRP, and cyclic nucleotide-gated channels as well as ionotropic glutamate receptors. To analyze the structural features of the pore in detail, we leveraged the power of genetic selections in yeast to examine interactions between the channel and permeant ions by employing barium as a probe of the ion conduction pathway.

Results

Genetic Selections Identify Barium-Resistant Kir2.1 Channels

Rescue of the growth of potassium transport-deficient yeast by functional ion channels provides a facile genetic system for exploring channel structure-function relationships (Bichet et al., 2004; Minor et al., 1999; Sadja et al., 2001; Yi et al., 2001; Zaks-Makhina et al., 2004). As the first step in developing this system as a means to identify ion channel blockers and examine the details of ion channel-blocker interactions, we investigated the ability of the universal potassium channel pore blocker, Ba^{2+} (Armstrong and Taylor, 1980; Hille, 2001), to prevent rescue by Kir2.1 (Kubo et al., 1993) (Figure 1A). Barium and potassium have similar ionic radii (1.35 Å and 1.33 Å, respectively), a physical similarity that has been exploited extensively to dissect potassium channel pore properties (Alagem et al., 2001; Hille, 2001; Neyton and Miller, 1988a, 1988b; Proks et al., 2003; Vergara et al.,

1999; Zhou et al., 1996). Under low potassium selection conditions, barium inhibited the growth of yeast requiring Kir2.1 for survival but not controls relying on the potassium transporter TRK1 (Gaber et al., 1988) (Figure1A), suggesting that this approach can detect channel blockers. Selection experiments using a library of Kir2.1 pore region mutants identified three independent barium-resistant mutants (P-Ba#1, P-Ba#2, and P-Ba#3) that rescued growth on limiting potassium in the presence of blocker (Figure 1B). Two-electrode voltage-clamp (TEVC) experiments in *Xenopus* oocytes revealed that these mutants produce inwardly rectifying potassium channels (Figure 1C) with significantly reduced barium affinities (~40- to 50-fold change at −80 mV, $Kd_{-80\ mV}$ = 6.5 ± 0.3, 305 ± 20, 264 ± 18, and 352 ± 20 μM for Kir2.1, P-Ba#1, P-Ba#2, and P-Ba#3, respectively) (Figure 1D). The similar affinity changes indicate that the shared mutation, T141K, which occurs at a residue known to contribute to Kir barium sensitivity (Alagem et al., 2001; Proks et al., 2003; Zhou et al., 1996), is largely responsible for the channel's acquired resistance to barium block.

How does the T141K mutation confer barium resistance? T141K resides at the first position of the highly conserved potassium channel selectivity filter signature sequence, "TTxGYG" (Heginbotham et al., 1994) (Figure 2A). Potassium channel selectivity filters have four ion binding sites (Aqvist and Luzhkov, 2000; Berneche and Roux, 2001; Zhou et al., 2001). Barium binds preferentially to the innermost site, "site 4" (Jiang and MacKinnon, 2000). Although there are important structural differences between Kirs and the bacterial channel KcsA (Bichet et al., 2003; Kuo et al., 2003; Minor et al., 1999), the strong conservation of the residues that make the selectivity filter suggests that the barium binding sites are similar. Modeling the equivalent selectivity filter change in KcsA (T74K) suggests that the lysine ζ-amino group could approach within ~5 Å of the site 4 ion and that our counterselection approach identified a mutation that acts through a direct electrostatic interaction with the blocking ion. These results highlight the potential power of the yeast selection system to identify ion channel blockers and map their modes of action.

Electrostatic interactions between the pore helix dipole and permeant cations have been proposed to stabilize ions as they transit the channel, even though the dipole's negative end is farther from the permeant ions (~8 Å) than would normally permit a meaningful charge-dipole electrostatic interaction (Doyle et al., 1998; Roux and MacKinnon, 1999). Given this model, it was striking that mutants that should effectively cancel the stabilization afforded by the pore helix by placing formal positive charges at its negative end (Figure 2B) passed the selection and were functional (Figure 1).

Characterization of T141 Substitutions on Barium Block and Ion Permeation

To examine further the effects of changes at the pore helix C terminus, we characterized a series of point mutations that alter residue charge and sidechain volume (T141R, T141H, T141E, T141D, T141M, T141Q, and T141S) (Figures 3A and 3B). All except for T141D produced functional channels. None of the functional mutants exhibited significant alteration in ion selectivity (see Figure S1 in the Supplemental Data available online). Comparison of barium blocking affinities suggests that two components lower barium affinity: a steric component, as exemplified by T141M and T141Q, and an electrostatic component. Formally positively charged changes T141K and T141R cause similar effects and are more barium resistant than the neutral, isosteric T141M. In contrast, the formally negatively charged mutant, T141E, binds barium tighter than the neutral, isosteric substitution T141Q (Figures 3A and 3B). When compared to neutral replacements of similar sidechain shape and volume, the effects of T141K, R, and E substitutions clearly follow the predicted direction for an electrostatic effect: tighter barium binding when position 141 is negative and weaker barium binding when position 141 is positive. Analysis of the blocking rates (Figures 3C and 3D) shows that all perturbations produce similar effects on k_{on}, whereas k_{off} is sensitive to the formal charge (T141R ≈ T141K ≫ T141M ≈ T141Q > Kir2.1 ≈ T141E). Together, these

data suggest that the presence of a charged mutation near the blocking site is key for affecting barium affinity.

Structural studies indicate that during normal channel operation site 4 binds potassium ions as they traverse the selectivity filter (Zhou et al., 2001). Reduction in the ion occupancy at site 4 has been shown to cause a significant loss (~8-fold) in single-channel conduction properties (Zhou and MacKinnon, 2004). Therefore, the electrostatic perturbations at site 4 that alter barium binding might also affect potassium permeation. We compared the single-channel conductances of T141K, T141R, T141M, and T141E to wild-type channels (Figures 4A and 4B). Remarkably, neither T141K nor T141R impact ion permeation significantly (γ = 22.4, 18.2, and 16.6 pS for Kir2.1, T141K, and T141R, respectively). Analysis of Kir2.1 and T141K single-channel conductance as a function of potassium concentration (Figure 4C) further underscores the similarity between T141K and wild-type permeation properties (K_m = 104 ± 7, 78 ± 11, γ_{max} = 48 ± 1, 36 ± 2 for Kir2.1 and T141K, respectively).

Physiologically, outward currents through Kir2.1 channels are blocked by the binding of cytoplasmic polyamines and magnesium to the channel interior (Lu, 2004). Because the electrostatic perturbation by T141K might affect outward movement of permeant ions, we examined T141K outward currents in excised macropatch experiments where the intracellular blockers were absent. In excised patches, T141K channels show linear responses to changes in membrane voltage. These results exclude the possibility that the T141K ζ-amino group acts as a tethered blocker that could affect outward current (Figure 4D). When 100 μM spermidine was applied to the intracellular side of the patch, T141K outward currents were blocked in a similar manner to wild-type channels (data not shown). Taken together with the potassium permeation similarities of T141K and wild-type channels as a function of potassium concentration, the lack of an effect on outward current further excludes the possibilities that the potassium occupancy at site 4 is greatly reduced by the T141K change and that a significant barrier to potassium ion entry into site 4 has been introduced by the mutation. In contrast, a mutation at the adjacent conserved selectivity filter threonine (TTxGYG) in KcsA, T75C (equivalent residue to Kir2.1 T142), removes the sidechain oxygen atoms that are involved directly in site 4 ion coordination and causes a substantial reduction in single-channel conduction accompanied by reduced ion occupancy at site 4 (Zhou and MacKinnon, 2004). Finally, excised macropatch experiments using bi-ionic conditions (Figure 4D) show that the T141K mutation causes no difference in permeant ion selectivity relative to wild-type channels (P_{Rb}/P_K = 0.53 ± 0.03 and 0.52 ± 0.09 for Kir2.1 and T141K, respectively). Collectively, our experiments strongly suggest that potassium ions are largely blind to electrostatic perturbations at the C-terminal end of the pore helix.

Acidic Residues within the Channel Cavity Support T141K and T141R Mutations

Functional studies suggest that the Kir2.1 T141 position is accessible to permeant ions (Kubo et al., 1998). Modeling T141K and T141R substitutions into the KirBac1.1 (Kuo et al., 2003) and KcsA (Doyle et al., 1998) structures supports the notion that the sidechain charges are near the C-terminal end of the pore helix in the channel's central cavity. Alternative sidechain conformations that do not place the charged terminus of the sidechain in the channel cavity require substantial disruption of the selectivity filter, which would be inconsistent with our functional data showing little change in ion selectivity or permeation between wild-type and mutant channels. How could four formally positively charged residues exist in proximity within the channel lumen? The negatively charged residue D172 resides on the channel lumen face of the pore-lining helix M2 (Kuo et al., 2003; Minor et al., 1999) and could interact with and support the presence of the T141K and T141R sidechain charges in the cavity. The neutral, isosteric single mutant D172N is functional (Lu, 2004); however, we found that the double mutants T141K/D172N and T141R/D172N were not

(data not shown). Similarly, a mutation that changed sidechain length but preserved the charge D172E but not the isosteric neutral mutation D172Q was compatible with T141K and T141R (Figures S2A and S2B). These results suggest that residues at 141 and 172 interact in a way that might be electrostatic and that interaction of the T141K and T141R positive charges with the helix dipoles alone offers insufficient stabilization. Kir2.1 residues 165, 169, 172, and 176 face the pore and tolerate a range of amino acid changes, including simultaneous substitution by aspartate (Minor et al., 1999). To test whether electrostatic interactions underlie accommodation of the T141K and R changes, we generated triple mutants that moved the negative charge along the M2 helix toward or away from T141K and T141R (T141K/S165D/D172N, T141K/C169D/D172N, T141K/D172N/I176D, T141R/S165D/D172N, T141R/C169D/D172N, and T141R/D172N/I176D). Although functional on its own (Figure S2c), S165D/D172N was incompatible with the additional T141K and T141R mutations (Figure 5A). Inspection of KirBac1.1 models suggests that there is insufficient room to accommodate T141K/S165D and T141R/S165D due to steric clashes between the mutated residues. Triple mutants with the M2 negative charge moved to positions 169 or 176 were functional (Figures 5B and 5D) and demonstrate that the precise geometry of the interaction between the positive charge at 141 and the negative charge in the cavity is not critical. These results support the idea that the T141K and T141R positive charges reside within the channel's central cavity, where they are stabilized by electrostatics.

To examine whether the requirement of T141K and T141R substitutions for a negative charge in the cavity led to a situation that would be functionally equivalent to a neutral cavity, we examined the effects on barium affinity resulting from the single pore-lining mutation D172N. The data show that D172N causes a small change in barium affinity (~4-fold at −80 mV, Figure 5E). This change is an order of magnitude smaller than those measured for the T141K and T141R substitutions the background of the wild-type D172. As a second control, we also examined the double mutant T141M/D172N. This mutant incorporates the neutral cavity together with a neutral residue at T141 that is isosteric to K and R. This mutant has a change in barium affinity that is also less than that seen for T141K and T141R (Figure 5E). Together, these results demonstrate directly that the necessary interaction between K or R at 141 and negative residues in the central cavity is not equivalent to channels with a neutral cavity. These data lend further support to the idea that the changes we observed in barium affinity arose from electrostatic perturbations at the end of the pore helix near selectivity filter ion binding site 4.

Continuum Electrostatic Calculations

Why are the forces that perturb barium binding only weakly sensed by potassium? We used macroscopic continuum electrostatic calculations and the KirBac1.1 structure to gain insight into this question. Here, the energy for ion transfer from solution to the binding site is $\Delta G(Q) = AQ^2/2 + BQ + C$, where Q is the ionic charge, $AQ^2/2$ is the ionic desolvation energy, BQ is the interaction between the ion and all protein charges, and C is a constant (Roux and MacKinnon, 1999; Zhou and MacKinnon, 2004). The calculations suggest that the energetics for transfer of a potassium ion to any of the four binding sites in the selectivity filter of KirBac1.1 is similar (Figure 6A). In contrast, the energetics of transfer of barium into site 4 are greatly favored over transfer to sites 1 through 3 (Figure 6A). The energetic preference of barium site 4 over the other sites agrees with experimental observations that barium is favored at site 4 over potassium (Jiang and MacKinnon, 2000; Neyton and Miller, 1988a, 1988b). Site 4 is the only position where both selectivity filter backbone carbonyl and threonine sidechain oxygen atoms coordinate the ion (Zhou and MacKinnon, 2004) and where the ion is partly solvated by the water in the channel cavity, a feature that appears to underlie its barium preference.

Figure 6B evaluates the effects of the electrostatic contribution of components of the KirBac1.1 structure as well as charge mutations at the 141 equivalent site and the M2 sites. Calculations suggest that the pore helix may contribute electrostatic stabilization at site 4 that largely originates from the partial charges of the free carbonyl groups in the last turn (cf. Aqvist et al., 1991; Roux and MacKinnon, 1999). Inclusion of a positive charge at the T141 equivalent (A109) destabilizes potassium and barium at site 4. Further inclusion of cavity-lining negative charges at experimentally compatible positions (KirBac1.1 M135, I138, and T142, equivalent to Kir2.1 169, 172, and 176) reduces the potassium transfer energy to near zero, but still disfavors barium (Figure 6B). Calculations with a model of an open channel, MthK, (Figure S3b) show a similar trend for site 4: destabilization by lysine substitution that can be compensated by negative residues on the pore-lining helices. It should be noted that analysis of MthK-derived models are limited because of the large degree of uncertainty in the models (Figure S3, see legend).

Although limits in both the calculations and models (Allen et al., 2004) preclude a detailed interpretation of ion permeation energetics, the qualitative agreement with our experimental observations further supports an electrostatic origin for the observed experimental effects. Evaluation of the relative contributions of the terms indicates that barium is more sensitive than potassium because changes in the BQ term, the electrostatic component, cause a loss of compensation for the larger dehydration penalty incurred by the $AQ^2/2$ term (Table S1).

Discussion

Ion channel proteins are essential membrane components for electrical signal generation and propagation in both excitable and nonexcitable cells (Hille, 2001). A central property of all ion channels is their ability to facilitate ion passage across the cell membrane at rates near the diffusion limit (Berneche and Roux, 2001, 2003; Hille, 2001). Of the many classes of ion channels, potassium channels constitute the best-studied subtype (Jan and Jan, 1997). These channels are remarkable devices that exhibit the properties of high ion throughput and high ion selectivity. While the basic architecture that gives rise to these properties is known (Doyle et al., 1998; Zhou et al., 2001), fundamental questions remain about how ion permeation is energetically tuned.

Understanding and identifying ion channel-blocker interactions also remains a major challenge with implications for both basic research and the development of new channel-directed pharmaceuticals. Because of their transmembrane environment, ion channels have been largely refractory to high-throughput approaches that have worked so well to identify such agents for soluble proteins (Numann and Negulescu, 2001). Thus, many ion channels lack any significant pharmacological agents that could be used to control and probe their function. Our experiments underscore the utility of using genetic selection approaches as an unbiased way to identify channel blockers and to identify and study channel elements that are important for the energetics of ion channel-blocker interactions.

Potassium channel permeation has been described as a cycle in which pairs of ions move between isoenergetic selectivity filter binding sites (1,3 4 2,4) as new ions enter the queue (Aqvist and Luzhkov, 2000; Berneche and Roux, 2001, 2003; MacKinnon, 2004; Morais-Cabral et al., 2001; Zhou et al., 2001). Site 4's avidity for barium leads to block (Jiang and MacKinnon, 2000). Introduction of the positive charge near site 4 raises the electrostatic energy of barium and potassium to different degrees (Figures 6C and 6D) and raises the barrier to the movement of ions from other configurations into site 4. The small perturbation of site 4 for potassium is consistent with two experimental observations: a lower saturation value for the channel and a modestly reduced single-channel conductance (Figure 4C). The former likely results from the reduction in isoenergetic states in the filter, while the latter

results from the introduction of a small barrier to ion flux. The larger change in barium binding energy results in channels that bind barium more weakly than wild-type.

Structural studies of potassium (Doyle et al., 1998) and chloride channels (Dutzler et al., 2002) suggested a unified mechanism for permeant ion stabilization despite the opposite ion charges and dissimilar channel architectures. Both channel types aim pore helix termini toward the permeant ions in a manner that matches the helix dipole end with the permeant ion charge (Dutzler et al., 2002). In potassium channels, the pore helix C-terminal carbonyls are far from the permeant ions (~8 Å), whereas in chloride channels, permeant ions contact the amides of the pore helix N terminus directly (Dutzler et al., 2002). The importance of helix macrodipoles in proteins remains unknown (Nakamura, 1996). Model system experiments failed to find the length dependence that should be associated with a helix macrodipole (Lockhart and Kim, 1992). Moreover, computational and experimental studies suggest that any electrostatic effects arise largely from the unpaired hydrogen bonding groups near the termini (Aqvist et al., 1991; Sitkoff et al., 1994) that act over very short distances (Aqvist et al., 1991; Miranda, 2003) and not the helix macrodipole. Our data strongly suggest that any interactions between permeant ions and the potassium channel pore helix have minimal effects on the energetics of ion permeation.

Pore helix dipoles have been principally invoked to explain the presence of an ion the KcsA cavity that lacks direct interactions with the protein (Roux and MacKinnon, 1999). There is no high-resolution structure currently available for Kir2.1, and its bacterial homolog, KirBac1.1, does not have a cavity ion. The absence of the cavity ion in the KirBac1.1 structure may be due to the modest structural resolution or the conformational state represented in the crystal (Kuo et al., 2003). Continuum electrostatic calculations suggest that a KirBac cavity ion could be stabilized similarly to that seen in KcsA, as the KirBac pore helices similarly point into the channel cavity, albeit with a slightly different alignment (Faraldo-Gomez and Roux, 2004). Smaller contributions to cavity ion stabilization may be made by the pore helix in open-state channels (compare Figure 6B and Figure S3b). Regardless of the precise geometry of the pore helices, it should be noted that the cavity ion is less influenced by the pore helices than the site 4 ion (Figure S3a). It remains possible that Kir channels are less sensitive to pore helix effects than other types of potassium channels.

Our data suggest that the inner vestibule of the potassium channel selectivity filter withstands dramatic changes in local electrostatics without major compromise of function. Regardless of whether the positively charged barium-resistant mutants counteract the helix dipole or mask the partial charges at the C-terminal end of the helix, the data indicate that electrostatic perturbations near the internal side of the selectivity filter have minor effects on potassium throughput. Thus, despite the aesthetic appeal of prior models, any contribution to ion permeation from the pore helices must be small.

Experimental Procedures

Random Library Construction and Genetic Selections

A Kir2.1 P-region library covering residues 128–143 was constructed using methods similar to those described previously (Minor et al., 1999). Site-directed mutagenesis was used to remove the PvuI site from residue 142 and reintroduce it at residue 155 by silent mutations that preserved the wild-type amino acid sequence. The coding DNA between BglII and PvuI was replaced by a non-coding “stuffer” sequence (Minor et al., 1999) to make a nonfunctional background for library construction.

A P-region cassette was synthesized by PCR of overlapping oligonucleotides (Biosynthesis, Houston, TX) in which the bases for amino acids 128–143 contained 91% of the wild-type

base and 3% each of the other three bases, yielding an average of 3.8 codon changes per sequence. DNA sequencing of 76 unselected clones showed that library members contained 3.3 amino acid changes per sequence on average. Position T141 was changed to 12 different amino acids in this random pool, showing good sequence coverage.

Genetic selections using potassium transport-deficient yeast were done as previously described (Minor et al., 1999). Immediately following replica-plating from high potassium (100 mM KCl) to low potassium (1 mM or 0.5 mM KCl) plates, 1 cm filter discs (Whatman, part number 1823010) soaked with 100 μl of 100 mM or 10 mM $BaCl_2$ were applied, respectively. Yeast were grown at 30°C for 2–3 days. Barium-resistant clones were chosen from the colonies growing near the filter. Plasmid DNA was recovered, and the phenotype was verified by retransformation and rescreening.

Electrophysiology

Constructs for electrophysiology were subcloned into a pGEMHE derivative (Minor et al., 1999); RNA transcripts were made using the Ampliscribe kit (Epicentre Technology) and were injected into *Xenopus* oocytes as described (Alagem et al., 2001; Minor et al., 1999). Two-electrode voltage-clamp experiments were performed using a GeneClamp 500B (Axon Instruments) amplifier using previously described protocols (Alagem et al., 2001; Minor et al., 1999) and digitized at 1 kHz with a Digidata 1332A (Axon Instruments) on cells expressing <5 μA of inward current at −100 mV in recording solutions of 90 mM KCl (Suprapur grade, EM Science), 2 mM $MgCl_2$, and 10 mM HEPES (pH 7.4), adjusted with KOH. For barium affinity measurements, the preceding solution was supplemented with different concentrations (from 0.5 nM to 50 mM) of $BaCl_2$. Perfusion was controlled using a Valvelink 16 (AutoMate Scientific) controller. k_{on} was determined from the concentration dependence of the observed blocking rates as described (Alagem et al., 2001). k_{off} was obtained using the relation $k_{off} = k_{on} \times Kd$. For single-channel and macropatch experiments, currents were measured by the patch-clamp technique (Hamill et al., 1981) in either cell-attached or inside-out configurations, using an Axopatch 200B amplifier (Axon Instruments). The currents were digitized at 5 kHz using Digidata 1200B (Axon Instruments) and low-pass filtered at 1 kHz using an 8-pole Bessel filter (Frequency Devices). For single-channel recording, pipettes were coated with Sylgard (Corning) prior to fire polishing. Pipettes were modified for macropatch recordings as described previously (Reuveny et al., 1996). Pipette solution for single-channel recordings contained 45, 90, 150, or 300 mM KCl, 10 mM HEPES, 2 mM $MgCl_2$, and 0.05 mM $GdCl_3$ (pH 7.4). The 45 mM KCl solution contained in addition 45 mM NMDG. For selectivity measurements, the pipette solution contained 150 mM KCl, 2 mM $MgCl_2$, and 10 mM HEPES (pH 7.4). The internal solution contained 150 mM KCl or 150 mM RbCl, 10 mM EDTA, 1 mM EGTA, and 10 mM HEPES (pH 7.4) (adjusted with either KOH or RbOH).

Electrostatic Calculations

Electrostatic interactions were calculated using the macroscopic continuum model with the program Delphi (Rocchia et al., 2002). Since the Kir2.1 structure is unknown, channel tetramers based on the X-ray crystal structures of KirBac1.1 (Kuo et al., 2003) and KcsA (Zhou et al., 2001) were used. Water molecules and Fabs were deleted from the structures. Calculations were also carried out using MthK structure, which is assumed to be in the open state. The side chains for the transmembrane domain of MthK, which are not resolved in the crystal structure, were built using the SWISS-MODEL program (Schwede et al., 2003). To simulate the experimental effects of the various mutations, the corresponding residues were manually built into the structures. A 24 Å thick slab of low dielectric consisting of dummy carbon atoms surrounding the protein was added to simulate the effect of the hydrophobic lipid bilayer.

Calculations were carried out with dielectric constant of protein and lipid at both 2 and 4 while the dielectric constant for the aqueous solution was 80. Hydrogens in the standardized geometry were added using Reduce (Word et al., 1999). Partial charges were assigned using the CHARMM parameters (Brooks et al., 1983). Ionic radii were the corrected Born radii (Rashin and Honig, 1995). In KirBac1.1, site 4 is not occupied. The location of this site was determined by superposing the selectivity filters of KirBac1.1 and KcsA. The reference energy state for the calculation is the protein-lipid complex without the cation at site 4, plus the cation dissolved in water.

Supplementary Material

Refer to Web version on PubMed Central for supplementary material.

Acknowledgments

The authors would like to thank A. Avelar for assistance with library construction; R.L. Baldwin, J.M. Berger, S. Boresch, K. Brejc, K.A. Dill, D. Fass, L.Y. Jan, E.A. Lumpkin, Z.-Y. Peng, P.A. Petillo, and N. Unwin for comments on the manuscript; and members of the Minor laboratory for support at all stages of this work. This work was supported by an award to E.R. and D.L.M. from the US-Israel Binational Science Foundation; to E.R. by the Israeli Science Foundation; and to D.L.M. from the PhRMA Foundation, AHA Western States Affiliate, Searle Scholars program, Rita Allen Foundation, Alfred P. Sloan Foundation, Beckman Foundation, Sandler Family Supporting Foundation, McKnight Foundation for Neuroscience, and the NIH. N.A. is supported by the Gina and Leon Fromer Endowed Postdoctoral Fellowship. D.L.M. is a Searle Scholar, a Rita Allen Foundation Scholar, an Alfred P. Sloan Research Fellow, and a Beckman Young Investigator.

References

Alagem N, Dvir M, Reuveny E. Mechanism of Ba(2+) block of a mouse inwardly rectifying K+ channel: differential contribution by two discrete residues. J Physiol 2001;534:381–393. [PubMed: 11454958]

Allen TW, Andersen OS, Roux B. On the importance of atomic fluctuations, protein flexibility, and solvent in ion permeation. J Gen Physiol 2004;124:679–690. [PubMed: 15572347]

Aqvist J, Luzhkov V. Ion permeation mechanism of the potassium channel. Nature 2000;404:881–884. [PubMed: 10786795]

Aqvist J, Luecke H, Quiocho FA, Warshel A. Dipoles localized at helix termini of proteins stabilize charges. Proc Natl Acad Sci USA 1991;88:2026–2030. [PubMed: 2000410]

Armstrong CM, Taylor SR. Interaction of barium ions with potassium channels in squid giant axons. Biophys J 1980;30:473–488. [PubMed: 6266531]

Berneche S, Roux B. Energetics of ion conduction through the K+ channel. Nature 2001;414:73–77. [PubMed: 11689945]

Berneche S, Roux B. A microscopic view of ion conduction through the K+ channel. Proc Natl Acad Sci USA 2003;100:8644–8648. [PubMed: 12837936]

Bichet D, Haass FA, Jan LY. Merging functional studies with structures of inward-rectifier K(+) channels. Nat Rev Neurosci 2003;4:957–967. [PubMed: 14618155]

Bichet D, Lin YF, Ibarra CA, Huang CS, Yi BA, Jan YN, Jan LY. Evolving potassium channels by means of yeast selection reveals structural elements important for selectivity. Proc Natl Acad Sci USA 2004;101:4441–4446. [PubMed: 15070737]

Brooks BR, Bruccoleri RE, Olafson BD, States DJ, Swaminathan S, Karplus M. CHARMM: a program for macromolecular energy, minimization, and dynamics calculations. J Comput Chem 1983;4:187–217.

Doyle DA, Morais Cabral J, Pfuetzner RA, Kuo A, Gulbis JM, Cohen SL, Chait BT, MacKinnon R. The structure of the potassium channel: molecular basis of K^+ conduction and selectivity. Science 1998;280:69–77. [PubMed: 9525859]

Dutzler R, Campbell EB, Cadene M, Chait BT, MacKinnon R. X-ray structure of a ClC chloride channel at 3.0 Å reveals the molecular basis of anion selectivity. Nature 2002;415:287–294. [PubMed: 11796999]

Faraldo-Gomez JD, Roux B. Electrostatics of ion stabilization in a ClC chloride channel homologue from Escherichia coli. J Mol Biol 2004;339:981–1000. [PubMed: 15165864]

Gaber RF, Styles CA, Fink GR. TRK1 encodes a plasma membrane protein required for high-affinity potassium transport in Saccharomyces cerevisiae. Mol Cell Biol 1988;8:2848–2859. [PubMed: 3043197]

Hamill OP, Marty A, Neher E, Sakmann B, Sigworth FJ. Improved patch-clamp techniques for high-resolution current recording from cells and cell-free membrane patches. Pflugers Arch 1981;391:85–100. [PubMed: 6270629]

Heginbotham L, Lu Z, Abramson T, MacKinnon R. Mutations in the K+ channel signature sequence. Biophys J 1994;66:1061–1067. [PubMed: 8038378]

Hille, B. Ion Channels of Excitable Membranes. Third. Sunderland, MA: Sinauer Associates, Inc.; 2001.

Jan LY, Jan YN. Cloned potassium channels from eukaryotes and prokaryotes. Annu Rev Neurosci 1997;20:91–123. [PubMed: 9056709]

Jiang Y, MacKinnon R. The barium site in a potassium channel by x-ray crystallography. J Gen Physiol 2000;115:269–272. [PubMed: 10694255]

Jiang Y, Lee A, Chen J, Cadene M, Chait BT, MacKinnon R. Crystal structure and mechanism of a calcium-gated potassium channel. Nature 2002;417:515–522. [PubMed: 12037559]

Jiang Y, Lee A, Chen J, Ruta V, Cadene M, Chait BT, MacKinnon R. X-ray structure of a voltage-dependent K+ channel. Nature 2003;423:33–41. [PubMed: 12721618]

Kandel, ER.; Schwartz, JH.; Jessel, TM. Principles of Neural Science. Fourth. New York: McGraw-Hill; 2000.

Kubo Y, Baldwin TJ, Jan YN, Jan LY. Primary structure and functional expression of a mouse inward rectifier potassium channel. Nature 1993;362:127–133. [PubMed: 7680768]

Kubo Y, Yoshimichi M, Heinemann SH. Probing pore topology and conformational changes of Kir2.1 potassium channels by cysteine scanning mutagenesis. FEBS Lett 1998;435:69–73. [PubMed: 9755861]

Kuo A, Gulbis JM, Antcliff JF, Rahman T, Lowe ED, Zimmer J, Cuthbertson J, Ashcroft FM, Ezaki T, Doyle DA. Crystal structure of the potassium channel KirBac1.1 in the closed state. Science 2003;300:1922–1926. [PubMed: 12738871]

Lockhart DJ, Kim PS. Internal stark effect measurement of the electric field at the amino terminus of an alpha helix. Science 1992;257:947–951. [PubMed: 1502559]

Lu Z. Mechanism of rectification in inward-rectifier K+ channels. Annu Rev Physiol 2004;66:103–129. [PubMed: 14977398]

MacKinnon R. Potassium channels and the atomic basis of selective ion conduction (Nobel Lecture). Angew Chem Int Ed Engl 2004;43:4265–4277. [PubMed: 15368373]

Minor DL Jr, Masseling SJ, Jan YN, Jan LY. Transmembrane structure of an inwardly rectifying potassium channel. Cell 1999;96:879–891. [PubMed: 10102275]

Miranda JJ. Position-dependent interactions between cysteine residues and the helix dipole. Protein Sci 2003;12:73–81. [PubMed: 12493830]

Morais-Cabral JH, Zhou Y, MacKinnon R. Energetic optimization of ion conduction rate by the K+ selectivity filter. Nature 2001;414:37–42. [PubMed: 11689935]

Nakamura H. Roles of electrostatic interaction in proteins. Q Rev Biophys 1996;29:1–90. [PubMed: 8783394]

Neyton J, Miller C. Discrete Ba2+ block as a probe of ion occupancy and pore structure in the high-conductance Ca2+-activated K+ channel. J Gen Physiol 1988a;92:569–586. [PubMed: 3235974]

Neyton J, Miller C. Potassium blocks barium permeation through a calcium-activated potassium channel. J Gen Physiol 1988b;92:549–567. [PubMed: 3235973]

Noskov SY, Berneche S, Roux B. Control of ion selectivity in potassium channels by electrostatic and dynamic properties of carbonyl ligands. Nature 2004;431:830–834. [PubMed: 15483608]

Numann R, Negulescu PA. High-throughput screening strategies for cardiac ion channels. Trends Cardiovasc Med 2001;11:54–59. [PubMed: 11530293]

Parsegian A. Energy of an ion crossing a low dielectric membrane: solutions to four relevant electrostatic problems. Nature 1969;221:844–846. [PubMed: 5765058]

Proks P, Antcliff JF, Ashcroft FM. The ligand-sensitive gate of a potassium channel lies close to the selectivity filter. EMBO Rep 2003;4:70–75. [PubMed: 12524524]

Rashin AA, Honig B. Reevaluation of the Born model of ion hydration. J Phys Chem 1995;89:5588–5593.

Reuveny E, Jan YN, Jan LY. Contributions of a negatively charged residue in the hydrophobic domain of the IRK1 inwardly rectifying K+ channel to K(+)-selective permeation. Biophys J 1996;70:754–761. [PubMed: 8789092]

Rocchia W, Sridharan S, Nicholls A, Alexov E, Chiabrera A, Honig B. Rapid grid-based construction of the molecular surface and the use of induced surface charge to calculate reaction field energies: applications to the molecular systems and geometric objects. J Comput Chem 2002;23:128–137. [PubMed: 11913378]

Roux B, MacKinnon R. The cavity and pore helices in the KcsA K+ channel: electrostatic stabilization of monovalent cations. Science 1999;285:100–102. [PubMed: 10390357]

Sadja R, Smadja K, Alagem N, Reuveny E. Coupling Gbetagamma-dependent activation to channel opening via pore elements in inwardly rectifying potassium channels. Neuron 2001;29:669–680. [PubMed: 11301026]

Schwede T, Kopp J, Guex N, Peitsch MC. SWISS-MODEL: An automated protein homology-modeling server. Nucleic Acids Res 2003;31:3381–3385. [PubMed: 12824332]

Sitkoff D, Lockhart DJ, Sharp KA, Honig B. Calculation of electrostatic effects at the amino terminus of an alpha helix. Biophys J 1994;67:2251–2260. [PubMed: 7696466]

Vergara C, Alvarez O, Latorre R. Localization of the K+ lock-In and the Ba2+ binding sites in a voltage-gated calcium-modulated channel. Implications for survival of K+ permeability. J Gen Physiol 1999;114:365–376. [PubMed: 10469727]

Woodhull AM. Ionic blockage of sodium channels in nerve. J Gen Physiol 1973;61:687–708. [PubMed: 4541078]

Word JM, Lovell SC, Richardson JS, Richardson DC. Asparagine and glutamine: using hydrogen atom contacts in the choice of side-chain amide orientation. J Mol Biol 1999;285:1735–1747. [PubMed: 9917408]

Yi BA, Lin YF, Jan YN, Jan LY. Yeast screen for constitutively active mutant G protein-activated potassium channels. Neuron 2001;29:657–667. [PubMed: 11301025]

Zaks-Makhina E, Kim Y, Aizenman E, Levitan ES. Novel neuroprotective K+ channel inhibitor identified by high-throughput screening in yeast. Mol Pharmacol 2004;65:214–219. [PubMed: 14722253]

Zhou M, MacKinnon R. A mutant KcsA K(+) channel with altered conduction properties and selectivity filter ion distribution. J Mol Biol 2004;338:839–846. [PubMed: 15099749]

Zhou H, Chepilko S, Schutt W, Choe H, Palmer LG, Sackin H. Mutations in the pore region of ROMK enhance Ba2+ block. Am J Physiol 1996;271:C1949–C1956. [PubMed: 8997197]

Zhou Y, Morais-Cabral JH, Kaufman A, MacKinnon R. Chemistry of ion coordination and hydration revealed by a K+ channel-Fab complex at 2.0 A resolution. Nature 2001;414:43–48. [PubMed: 11689936]

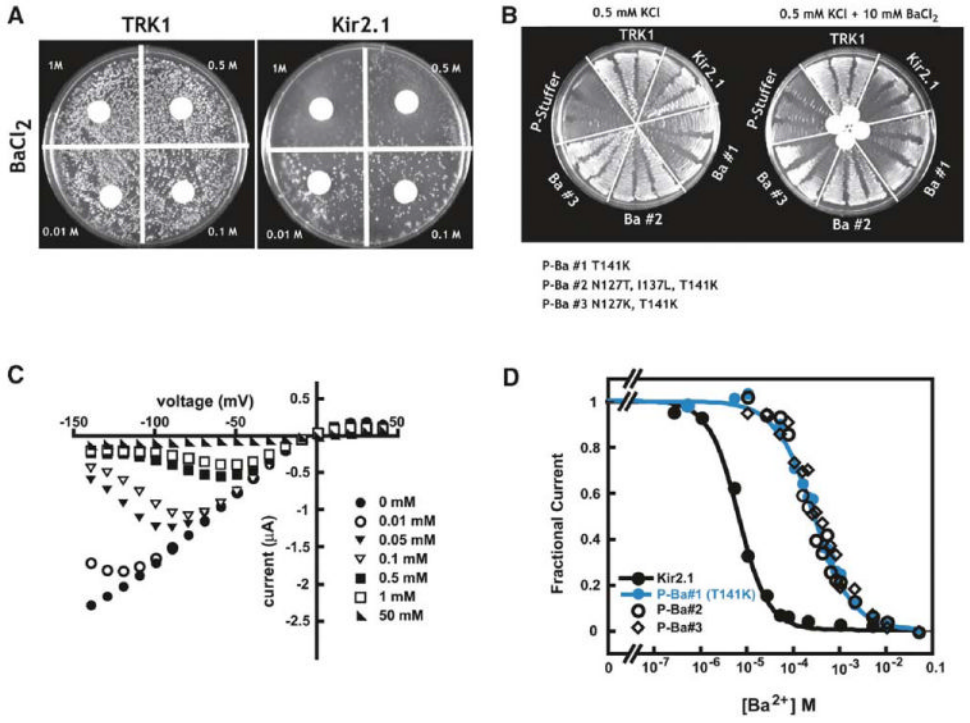

Figure 1. Genetic Selection for Channel Blockers and Characterization of Barium-Resistant Clones

(A) Effects of barium on the growth of yeast on selective media containing 0.5 mM KCl expressing the transporter TRK1 or the Kir2.1 potassium channel. Barium concentrations are indicated.

(B) Barium-resistant mutants rescue the transport-deficient phenotype on 0.5 mM KCl media in both the absence and presence of blocker.

(C) Current-voltage (I-V) relations for P-Ba#1 (T141K) in 90 mM KCl recording solution. Concentrations indicate the amount of barium present.

(D) Comparison of barium Kds at −80 mV for P-Ba#1 (T141K) (blue ●), P-Ba#2 (○), P-Ba#3 (◇), and wild-type Kir2.1 (●). Lines indicate fits to the Hill equation $I_f = Kd^n/(Kd^n + [Ba^{2+}]^n)$.

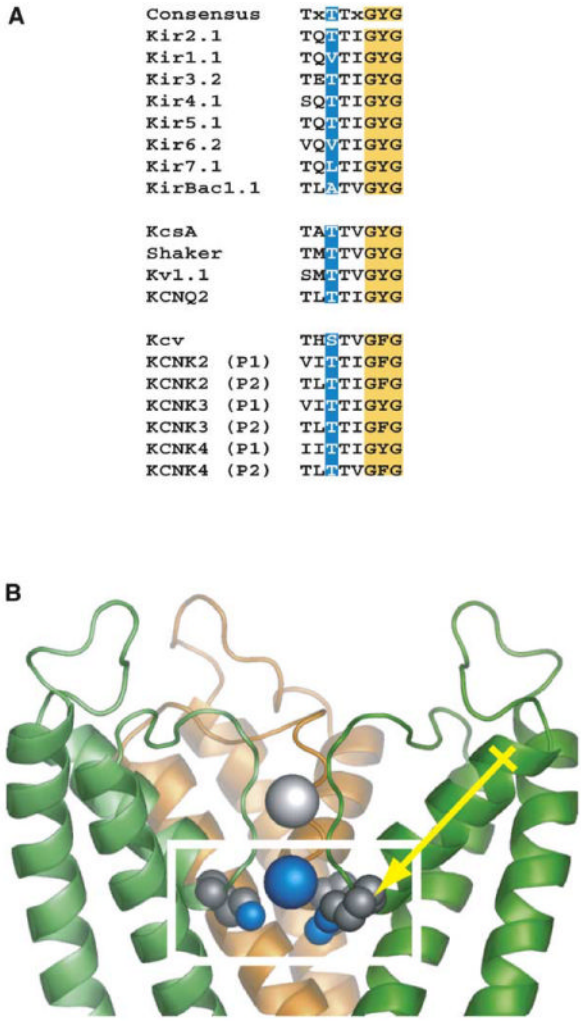

Figure 2. Location of T141

(A) Comparison of the selectivity filter sequences from each of the three major potassium channel families, inward rectifiers (Kir), voltage-gated channels, and Two-P (KCNK) channels. The conserved, T141-equivalent position is highlighted in blue.

(B) Model of the proximity of T141K to the barium blocking site using KcsA (Zhou et al., 2001). The box highlights the site of barium binding. The site 4 ion is shown as a blue sphere. The T141K mutation is shown in CPK. The expected direction of the pore helix dipole is shown for the right-hand subunit.

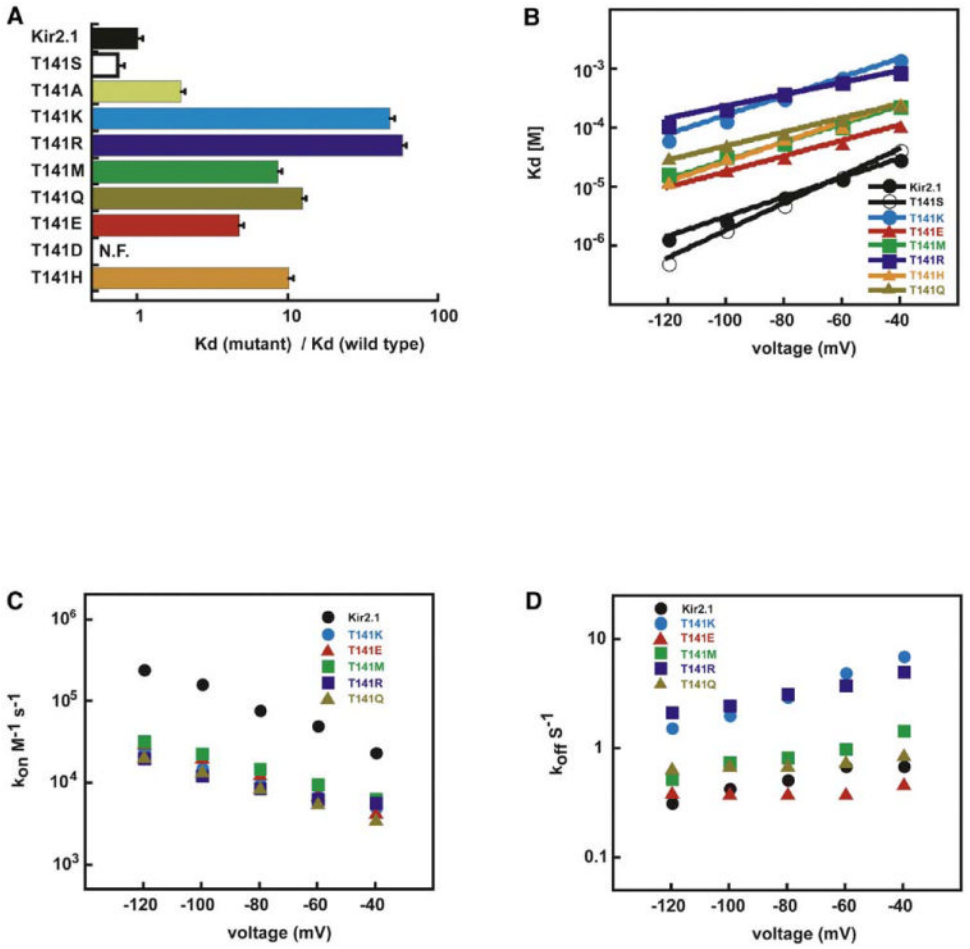

Figure 3. Kir2.1 T141 Mutant Channel Properties

(A) Comparison of relative barium dissociation constants of T141 mutant channels relative to wild-type and D172N at −80 mV. N.F., nonfunctional. T141A data are from Alagem et al. (2001). Error bars show standard deviations.

(B) Voltage dependence of steady-state barium block. Lines show fits to the Woodhull equation (Woodhull, 1973) $Kd(V) = Kd(0)\exp(zF\delta/RT \times V)$, Kd(0) values (μM) are as follows: Kir2.1, 131 ± 3; T141S, 349 ± 6; T141K, 6241 ± 468; T141R, 2218 ± 176; T141E, 362 ± 26; T141Q, 715 ± 40; T141H, 1199 ± 189; T141M, 934 ± 84. δ values are as follows: Kir2.1, 0.56 ± 0.02; T141K, 0.47 ± 0.02; T141R, 0.30 ± 0.02; T141E, 0.39 ± 0.04; T141Q, 0.35 ± 0.02; T141H, 0.50 ± 0.02; and T141M, 0.46 ± 0.02.

(C) k_{on} (M^{-1} s^{-1}) and (D) k_{off} (s^{-1}) for Kir2.1, T141R, T141K, T141E, and T141M. Throughout the figure, channels are denoted: Kir2.1 (black), T141S (open symbols), T141A (light green), T141K (blue), T141R (dark blue), T141M (green), T141E (red), T141Q (gold), and T141H (orange).

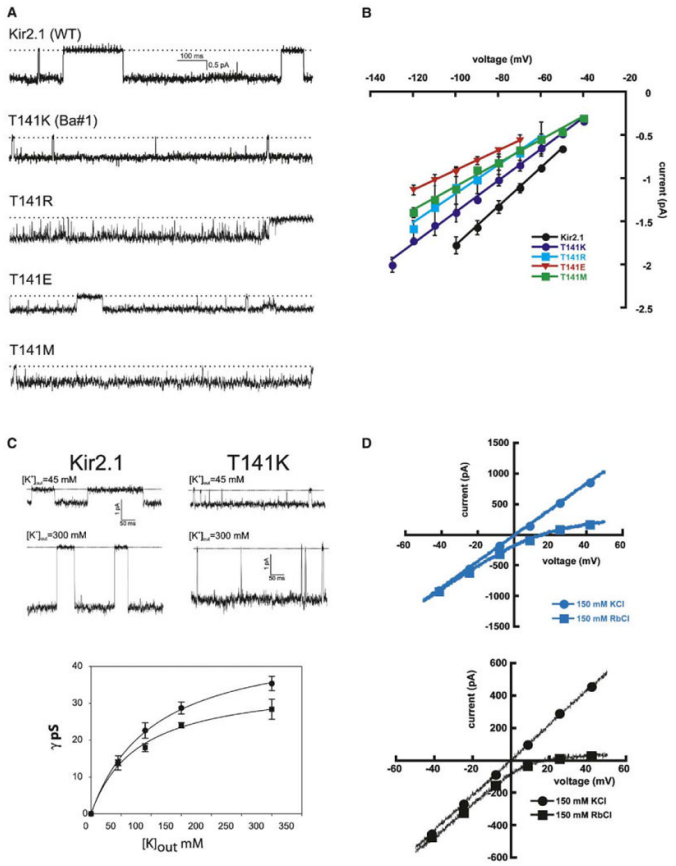

Figure 4. Comparison of Single Channel Properties of Kir2.1 and T141 Mutants

(A) Single-channel traces for Kir2.1, T141K, T141R, T141E, and T141M at −80 mV. The dotted lines denote the closed-state current levels. The T141M patch contained two channels.

(B) I-V plots for Kir2.1 (n = 3), T141K (n = 5), T141R (n = 9), T141E (n = 10), and T141M (n = 3). The lines are linear regressions, and the error bars show the standard deviations.

(C) (Top) Cell-attached single-channel records for Kir2.1 and T141K at −80 mV in the presence of different external potassium concentrations. (Bottom) Single-channel conductance as a function of $[K^+]$ out and Michaelis-Menten fits are indicated. Error bars show standard deviations.

(D) Comparison of I-V relations from inside-out excised macropatches of T141K (blue, top) and Kir2.1 (black, bottom) under either symmetrical 150 mM KCl (●) or the bi-ionic condition of 150 mM K^+ on the extracellular and 150 mM Rb^+ on the intracellular sides of the membrane (■). Data are from ramp protocols. Symbols are shown to guide the reader.

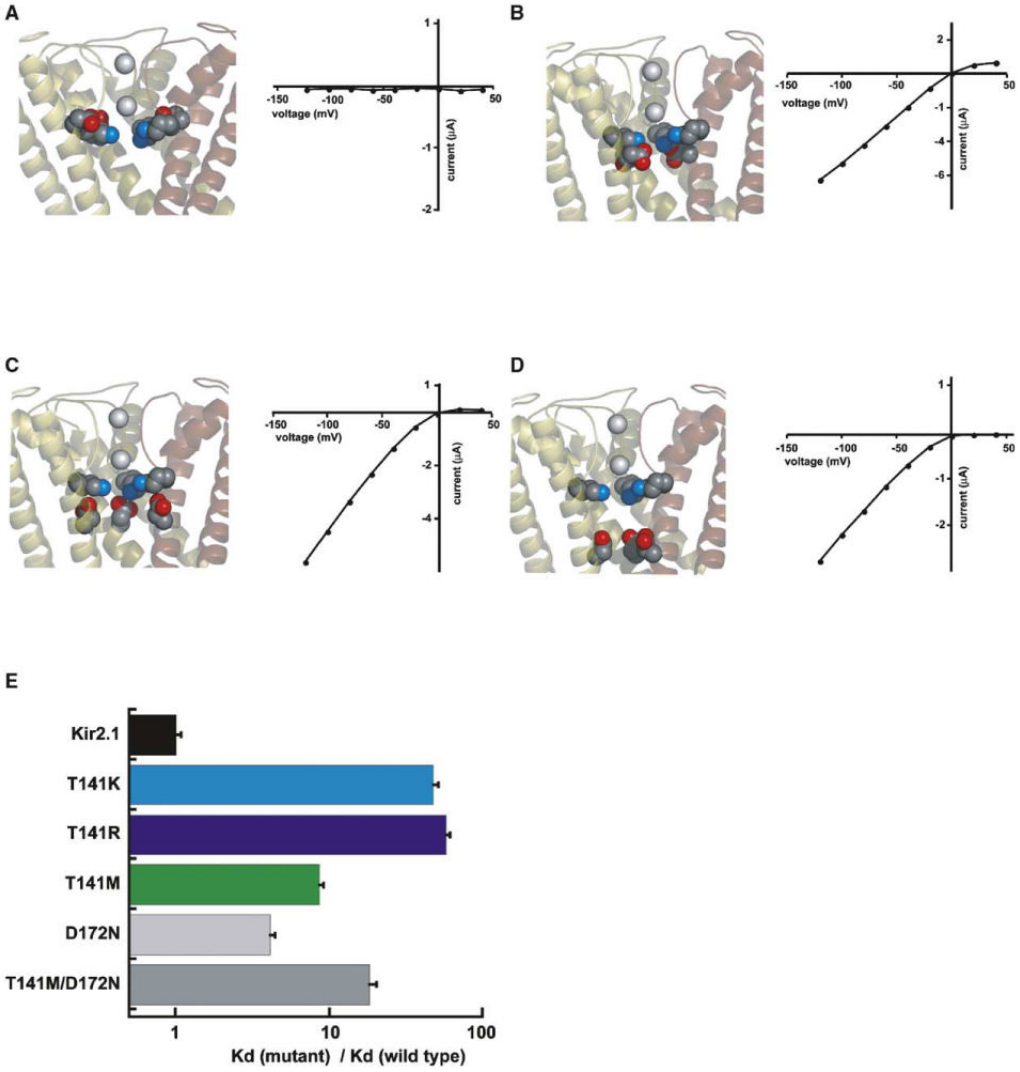

Figure 5. T141K Substitutions Require a Negative Charge in the Channel Cavity

(A–D) T141K substitutions require a negative charge in the cavity. Models are based on the KirBac1.1 structure with the position of T141K and the M2 acidic residue shown in CPK. I-V data and positions of the charged residues are shown for (A) T141K/S165D/D172N, (B) T141K/C169D/D172N, (C) T141K/D172, and (D) T141K/D172N/I176D. Similar results were obtained for the equivalent T141R mutants.

(E) Comparison of relative barium dissociation constants for channels with neutral cavities (D172N and T141M/D172N) and T141K, T141R, and T141M channels relative to wild-type at −80 mV.

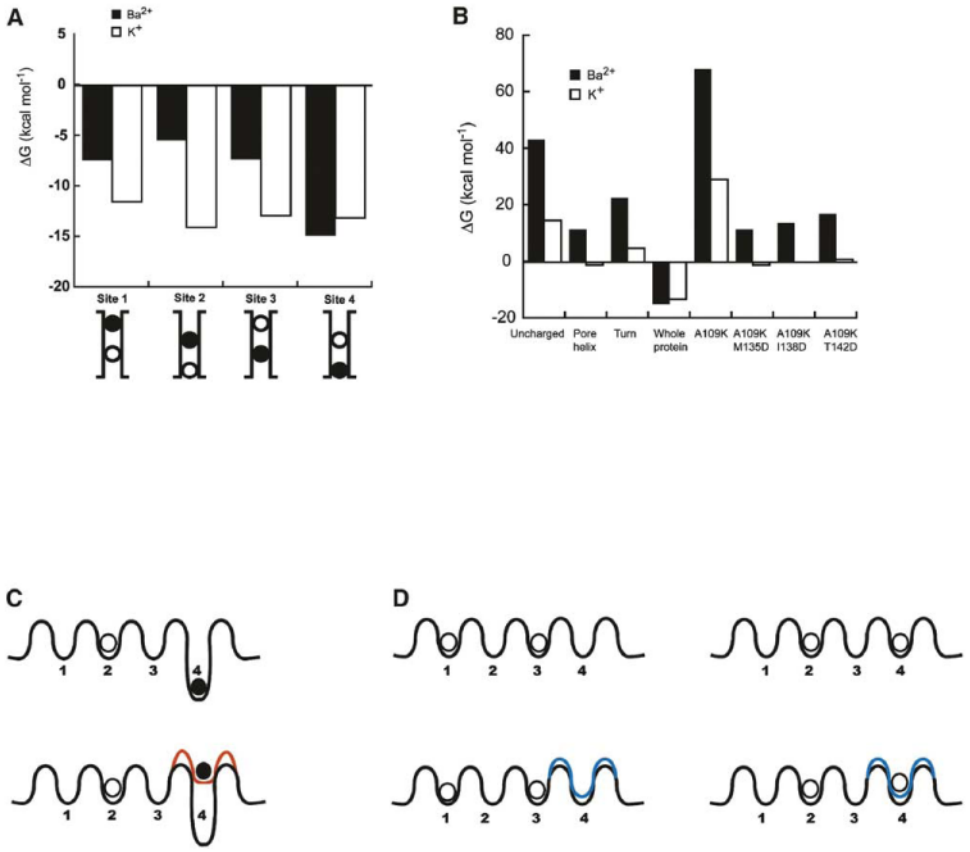

Figure 6. Evaluation of Changes to Selectivity Filter Energetics

(A) Comparison of the calculated changes in the free energy of transfer of Ba^{2+} (filled bars) and K^+ (open bars) to selectivity filter sites 1–4. Filter ion configuration is illustrated below the graph. The black circle depicts the site under investigation. The open circle represents the site of a second K^+ selectivity filter ion present in the calculation. Values result from calculations with $\varepsilon = 4$.

(B) Calculated changes in the free energy of transfer of Ba^{2+} (filled bars) or K^+ (open bars) from solution to site 4 in KirBac1.1 when site 2 is occupied by K^+. Energies are shown for conditions (left to right) with the uncharged protein, charges on pore helix residues 97–109 only, charges on the last turn of the pore helix only (residues A109, L018, T107, E106 [neutral form], and V105), charges on the whole protein, and the mutants A109K, A109K/M135D, A109K/I138D, and A109K/T142D in the background of the fully charged protein. Values result from calculations with $\varepsilon = 4$.

(C) Cartoon of the selectivity filter energy landscape for barium in wild-type and T141K or T141R mutants (red). Potassium ions are indicated as open circles, barium as black.

(D) Cartoon of the selectivity filter energy landscape for potassium in wild-type (black) and T141K or R mutants (blue). Potassium ions are indicated as open circles.